Proceedings of the ASME 2024
International Design Engineering Technical Conferences and
Computers and Information in Engineering Conference
IDETC2024
August 25–28, 2024, Washington, DC

DETC2024-143861

EXPERIMENTALLY SUPPORTED DESIGN OPTIMIZATION OF MARINE HYDROKINETIC TURBINE SYSTEMS WITH ADAPTIVE DUCT CONTRACTION CONTROL

Austin L. Griffin[1], Yong Hoon Lee[1,*]

[1]Department of Mechanical Engineering,
The University of Memphis, Memphis, TN

ABSTRACT

This study investigates a novel adaptive duct control strategy for maximizing power output in a ducted horizontal-axis hydrokinetic turbine (HAHkT) system. The strategy focuses on varying contraction ratios (CR) and rotor blade pitch angles to optimize energy production under specific inflow conditions. Experimental static data for three different CR and thirteen pitch angles are utilized to design and perform experiments aimed at creating a dynamic model tailored to the system's behavior.

Parametric analyses are conducted using QBlade software to assess rotor blade performance across various geometry configurations and flow conditions, with water as the medium. An open-channel water flume experiment is established to evaluate the performance of the small-scale ducted HAHkT with the selected range of CR and pitch configurations. The experimental data collected is utilized to construct a dynamic surrogate model (SM) capable of predicting system behavior. Optimizations tests controlling CR and blade pitch angle for maximal power extraction are performed with a variety of velocity profiles.

The proposed adaptive duct control strategy presents promising potential for developing highly efficient ducted HAHkT systems. By dynamically adjusting CR and pitch based on inflow conditions, this approach aims to achieve optimal energy production, ultimately contributing to the realization of cost-effective renewable energy solutions.

Keywords: horizontal-axis hydrokinetic turbine (HAHkT), ducted turbine, adaptive duct contraction control, experimentally supported design optimization

1. INTRODUCTION

As the global population continues to grow, so does the demand for energy, raising concerns regarding the sustainability and environmental impact of energy production [1, 2]. The heavy reliance on fossil fuels for energy generation has been linked to detrimental effects on the climate [3]. In response to these challenges, there has been significant effort to explore renewable energy sources, such as marine hydrokinetic turbines (HkTs), as viable alternatives to mitigate climate change [4, 5].

HKTs are classified into two primary groups based on the axis of rotation: horizontal-axis and vertical-axis turbines. Horizontal-axis hydrokinetic turbines (HAHkTs) have emerged as a promising avenue in the pursuit of renewable energy, offering advantages such as lower start-up speeds and higher output compared to their vertical-axis counterparts [6, 7]. However, achieving cost-efficient energy conversion in HAHkT systems necessitates a comprehensive optimization approach that encompasses various design parameters, including scale, external and internal geometry, rotor and blade design, and control schemes [8, 9].

Conventional design approaches encounter challenges due to the lack of validated, simple models appropriate for system-level optimization tasks. Existing models often rely on computationally-intensive computational fluid dynamics (CFD) simulations or limited reduced order models (ROMs), restricting their applicability across diverse flow conditions [10–12]. While ROMs offer computational efficiency, their effectiveness in dynamic system design optimization remains constrained by the complexity of the optimization problem [12, 13].

This study employs a series of numerical and experimental approaches for modeling a HAHkT system, and proposes a novel adaptive duct contraction control strategy along with blade pitch control to optimize the energy production for relatively low flow speed environments. We employed QBlade software integrated with Xfoil analyses to determine the optimal angle of attack for rotor blades. Following this initial step, Blade Element Momentum Theory (BEMT) simulations are conducted within QBlade to anticipate the coefficient of power for the designed rotor at various tip speed ratios, TSRs, and blade pitch angles. These

*Corresponding author: yhlee@memphis.edu

simulations form the basis for experimental design validation.

The experimental phase involves conducting tests in a recirculating open channel flume on duct contraction ratios (CRs) of 1, 0.75, and 0.5, alongside thirteen varied pitch angles. The purpose is to collect power output data, including voltage, current measurements, and rotor angular velocity (RPM), crucial for evaluating the system performance across various configurations. Following the experimental phase, the data undergo analysis using QBlade BEMT simulations. This analysis is intended to assess the system performance at the maximum power states associated with each CR. Specifically, this process involves investigating the hypothesis that a lower CR, which creates higher water velocity at the turbine rotor area, leads to increased power production.

The experimental dataset serves as the principle for constructing a surrogate model (SM). The HAHkT SM is creating using Kriging method included in the surrogate modeling toolbox (SMT) [14]. The developed SM represents dynamics of the HAHkT system behavior across varying conditions. Utilizing this SM, the optimal design solution for constrained and unconstrained cases across four distinctive water profiles emphasizes the adaptability and efficiency of the proposed HAHkT configuration and control strategy.

Novel contributions of this research are outlined as follows: (1) introducing an adaptive duct contraction control concept for HAHkT, (2) actively controlling both duct CR and rotor blade pitch to effectively harness energy from low water flow speeds, and (3) Integrating numerical and experimental processes in designing HAHkT systems, providing validated ROM for design exploration. With these novel contributions, we expect to offers a pathway to not only enhance the efficiency of HAHkT systems but also to realize cost-effective solutions for energy production, addressing the urgent need for sustainable energy technologies.

2. METHODS

This study emcompasses three primary research processes: experimental data generation, augmented simulation, and control strategy development.

In the experimental data generation process, a ducted HAHkT experimental apparatus is developed and utilized to conduct experiments in an open channel water flume. The HAHkT apparatus undergoes testing with varied combinations of rotor blade pitch angles and duct CRs under constant ambient flow speed conditions, yielding datasets of rotor rotational velocity and generator power output.

During the augmented simulation process, numerical models of the ducted HAHkT rotor blades are constructed using BEMT, followed by simulations to assess their performance, and compared with the experimental datasets obtained in the aforementioned process.

In the control strategy development process, an SM is constructed based on the experimental datasets representing the dynamic responses of the ducted HAHkT system. This SM is integrated into a design optimization formulation, where the blade pitch angle and duct CR values are simultaneously regulated to maximize power output while accommodating unsteady incoming ambient flow speed profiles. Subsequent sections provide detailed information of each of these three processes.

2.1 Numerical Analyses

The QBlade code, developed by TU Berlin, is used in this study for blade element momentum theory (BEMT) simulations to analyze turbine blades, incorporating specific airfoil geometries across distinct radial sections [15, 16]. Initially conceived for wind turbines, QBlade has proven its versatility by extending its functionality to the design of horizontal-axis hydrokinetic turbines (HAHkTs), leveraging its capabilities in aerodynamic and aero-elastic simulations [17].

Xfoil, alongside with QBlade, is utilized to obtain drag and lift coefficients across varied angles of attack (AoA, α) [15]. Xfoil analyses at specific Reynolds numbers are explored with respect to the root, middle, and tip of the blade. With this data then extrapolated, a comprehensive polar data set can be utilized for further simulations. Then, the subsequent 360° Viterna extrapolation is performed to fill the data in extreme AoA ranges for robust simulation. While BEMT provides detailed estimation of operational power generation of the designed rotor blades, Xfoil within QBlade allows a detailed examination of lift and drag coefficients, moment coefficients, and other aerodynamic characteristics across various airfoil cross-sectional profiles and AoA values. This two-step method is particularly useful when determining effective initial AoA across radial locations of the rotor blade, optimizing turbine performance by twisting the blade across its radius [18].

The power coefficient variations as a function of tip speed ratio (TSR) and collective pitch adjustments are predicted through BEMT simulations. These simulations provide a predictive framework before experimental design, allowing for informed decisions regarding rotor blade twist. Subsequently, during the post-experimental phase, QBlade's BEMT simulations are performed again to validate the power coefficient outcomes at maximum power for each duct CR value. This verification process confirms the effectiveness of the experimental design in achieving improved power coefficients, particularly for lower CRs.

The power coefficient for a particular turbine is determined with the expression:

$$C_P = \left(\frac{P_{\text{extracted}}}{P_{\text{available}}} \right). \tag{1}$$

The power coefficient, determined by the free stream velocity and the rotor area, complies with the Betz limit of 0.593 [17]. Correction for this power coefficient in relation to the entire ducted turbine is achieved through the following equation, given as [11]:

$$C_P^* = C_P \left(\frac{A_{\text{exit}}}{A_{\text{rotor}}} \right). \tag{2}$$

The power available for the fluid is then determined to be:

$$P_{\text{available}} = \frac{1}{2} \rho A_2 v_2^3, \tag{3}$$

following Refs. [12, 19]. Here, A_2 is the area at the rotor, consistently maintaining symbols from the earlier studies. With the power available and the power coefficient, the power extracted can be solved for and compared to experimental results.

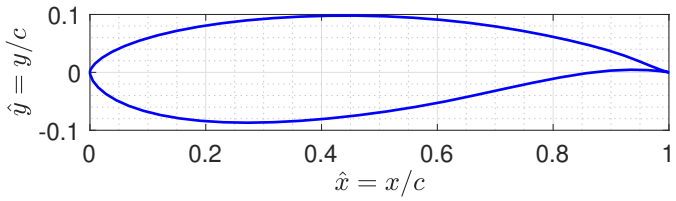

FIGURE 1: Normalized Profile of NREL S833 Hydrofoil

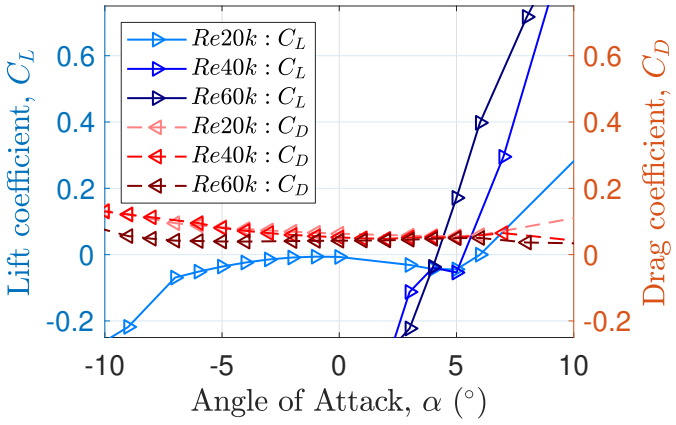

FIGURE 2: Lift and drag coefficients as functions of angle of attack at various Reynolds numbers

2.2 Experimental Setup

This experimental work utilizes a recirculating open channel flume to create controlled water flow along the axial direction of the HAHkT apparatus. The open channel is 4.42 meters long and was modified to include a 1.5 m wide insert, where the cross-sectional area of the flow reducing 240 mm by 275 mm, which is intended to increase the initial average velocity to 0.1 m/s. An initial test with the full flow directed through the turbine area provided a proof of concept and initial flow rate data necessary for performing more accurate simulations and therefore a better design. This maximized flow gave a Reynolds number near 60,000 at the tip of the blade. It is assumed that the water flow is incompressible and resides within the transitional regime, owing to the anticipated range of Reynolds numbers. While flow separation could potentially be observed at higher angles of attack, the operational range avoids the stall regime of the blade profile. The temperature of the flow for simulation purposes is considered to be a constant 20°C, however the experimental temperature was measured before and after each blade pitch test.

After the initial test was performed, the final designs of a ducted small-scale HAHkT were created for use in the open channel flume. These final designs comprised various components that were printed, constructed, and procured. The required equipment consisted of the following items and printed models: a brushed waterproof DC motor acting as a generator, a voltmeter to measure voltage, an ammeter to measure current, a flow meter to determine freestream flow speed, a high frame-rate camera to determine rotor angular velocity, a thermometer to monitor temperature fluctuations, thirteen different rotor models varying in collective pitch from −12° to +12° in increments of 2° , and three ducts with the duct CRs of 1, 0.75, and 0.5. For the rotor

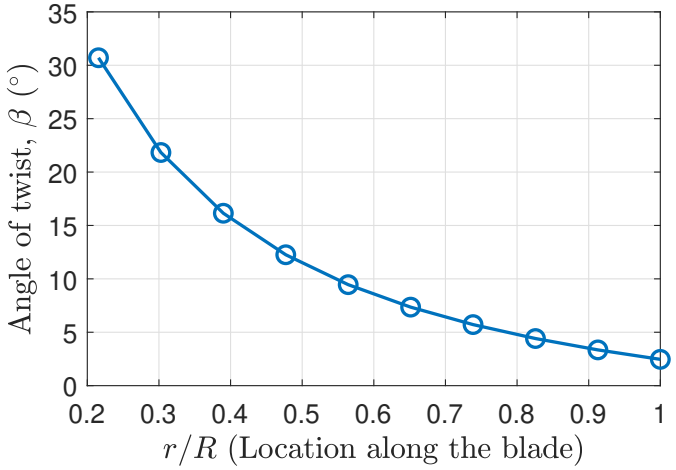

FIGURE 3: Angle of twist designed as a function of normalized radius along the blade

models, National Renewable Energy Laboratory (NREL) S833 hydrofoil blade profile was chosen as it demonstrated relatively higher performance in previous literature [20, 21].

The selected blade profile, NREL S833, is shown in Fig. 1. In order to find a suitable initial AoA, Xfoil analyses were performed in QBlade from −15° to +15° with a Reynolds numbers representing the root of the blade, the mid section of the blade, and the tip of the blade. The corresponding Reynolds numbers were rounded to the nearest 10, 000 to produce 20, 000, 40, 000, and 60, 000 respectively. The results for these analyses are shown in Fig. 2. From this figure it can be seen that certain points were not recorded due to stall. Previous work utilizing the NREL S833 at higher Reynolds numbers came to a conclusion that 6° is the ideal α [22]. However, in the figure it can be noted that the drag coefficient overtakes the lift coefficient at 6° for a Reynolds number of 20, 000 and therefore should be excluded. With this in mind the α of 7° was chosen as a baseline AoA (α_0) for the expected Reynolds number range. Figure 3 displays the angle of twist (AoT, β) for the idealized ducted rotor model. The AoT for the blade sections was calculated as:

$$\beta = \tan^{-1}\left(\frac{U}{r\omega}\right) - \alpha_0, \tag{4}$$

where U is the nominal velocity, which was initially set to 0.678 m/s, ω is the nominal rotational speed, which is set to 30.5 rad/s, and r is the distance along blade which began at a radius of 15 mm and increased by increments of 5 mm till the tip at 50 mm. This ensures that all local blade section locations have baseline angle of attack at the nominal flow speed and optimal tip speed ratio, TSR, when controlled blade pitch (θ_p) is maintained at 0°. The TSR of the initial test was on the lower end at 2.25. This was calculated as:

$$\text{TSR} = \left(\frac{r\omega}{U}\right). \tag{5}$$

Ducted hydrokinetic turbines operate more efficiently at higher TSR values than their bare counterparts [23, 24]. With this in mind, a TSR of 6 was selected as the idealized ducted TSR to which the β for the final rotor models would be based. U and

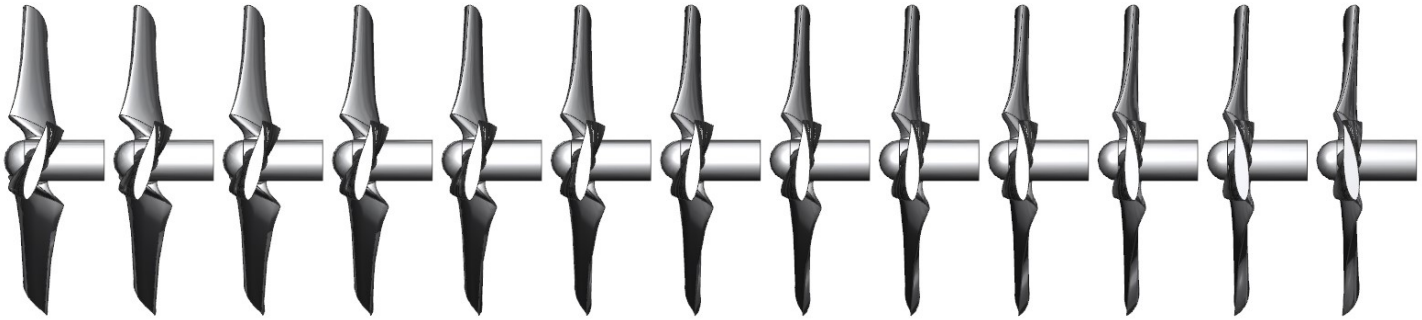

FIGURE 4: Three-dimensional Rotor Model Pitches from −12° to 12° in increments of 2°

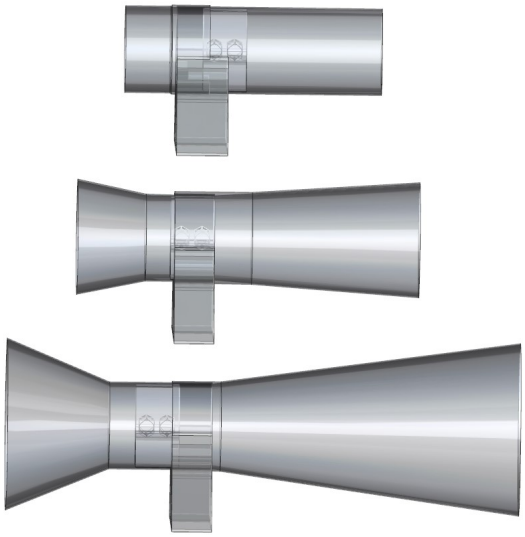

FIGURE 5: Duct configurations with duct CRs of 1, 0.75, and 0.5

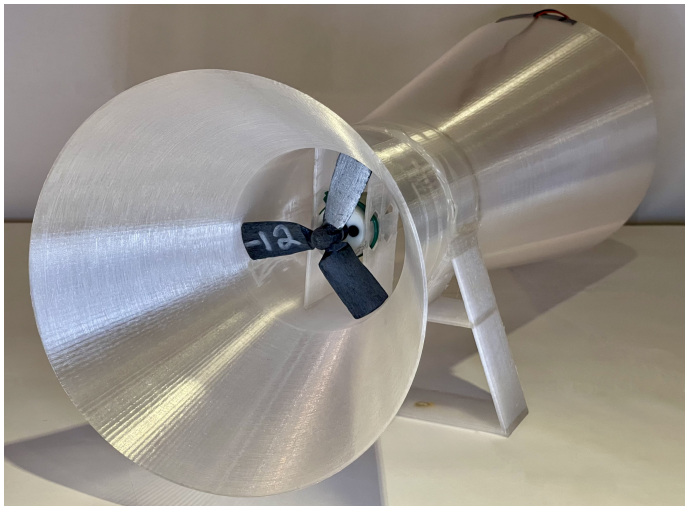

FIGURE 6: Experimental ducted HAHkT apparatus with duct CR=0.5 and −12° pitch rotor

ω were then set to 0.34 m/s and 40.8 rad/s respectively in order to produce this idealized TSR. Chord length was kept constant along the blade for experimental simplicity. Figure 4 shows the side view of all thirteen rotor models from pitch −12° to +12° in increments of 2°. Change in chord, tip clearance, cavitation, and the generator control were not explored in this research but are essential to incorporate for full control design optimization.

The thirteen different rotor designs, with each at a different fixed pitch, and three ducts of varying duct CRs were printed in the polymer Polyethylene terephthalate glycol, or PETG, via a fused material deposition, FDM, extrusion process. The Creality FDM printers utilized were the CR-M4 and the Ender V3 SE. The CR-M4 printed the duct pieces due to its relatively larger printing volume. However due to the length of the full ducts, each duct had to printed in two pieces. For the duct CRs of 0.5 and 0.75, the divergent nozzle was printed separately from the turbine area and divergent nozzle. Due to the reduction in total length for the duct CR of 1 and the fixed length of the rotor and the generator, the generator holder had to extend into the divergent nozzle such that the tip of the rotor wouldn't exceed the entrance of the convergent nozzle. Therefore, the convergent nozzle was printed separately from the turbine area and the divergent nozzle for the duct with the duct CR of 1. Both printers were utilized to print the rotor models at the thirteen different pitches. Figure 5 shows the final designs for each of the ducted assemblies printed and tested. In order to secure the duct assembly, the turbine base was screwed into anchor sockets on the base of the flume and the wire from the generator was secured to the divergent nozzle end and to the top wall of the flume, placing an upward force on the divergent end that counters the upward force on the convergent end from the incoming flow. The rotor pitch models were adhered with hot glue to a coupler located on the generator shaft. To change the rotor pitch model being tested, a heat gun was applied momentarily to the attached rotor to allow for the glue to melt and the rotor to be removed.

Lastly, the flow generated from the pumps was constant and therefore the flow was assumed to be steady. The primary objective for the experiment was to collect rotor rotational speed, output voltage, and output amperage data for various duct CRs and blade pitches. The output voltage and amperage were used to determine the average output power for all duct CR and blade pitch combinations. It is also possible to represent the measured electrical power output in terms of hydrodynamic efficiency. However, since we used a small DC motor as our power generator, which cannot produce sufficient resisting electromagnetic torque, the absolute electrical power values are more meaningful than the efficiency values. The free stream flow subsequent to the flow straightener and recording device but prior to the duct entrance

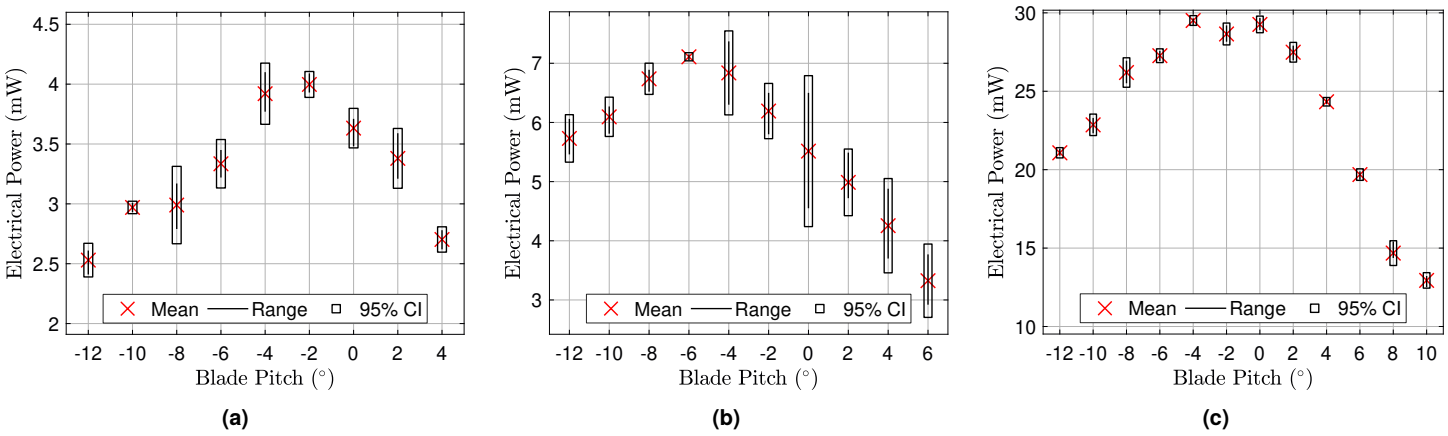

FIGURE 7: Experimental electrical power results as pitch and duct CR are varied. (a), (b), and (c) Individual power results for duct CRs equal to 1, 0.75, and 0.5.

was assessed with the flow meter before each pitch trial. The temperature data before and after each pitch trial is also recorded. This collection of data is essential in formulating the experimental power coefficient with the relationship in Eq. (1). Without any efficiency information, the power extracted is equated to the electrical output. Hydraulic power extracted from the water will be greater than the electrical power due to losses. The extracted power trends follow the same path at a reduced magnitude as pitch and duct CR are varied. These results are later compared to the simulated results and validity will be determined for optimal design parameters. The C_P can be corrected to find the power coefficient value associated with the entire duct, which abides by the Betz limit, using the same relationship previously mentioned in Eq. (2).

2.3 Adaptive Duct Contraction Control Optimization Plans

The next step in enhancing ducted HAHkT systems involves leveraging data from water flume experiments to develop an SM. This SM serves as a dynamic ROM, intricately designed to capture the complex interactions of varying duct CRs and blade pitch adjustments under different flow conditions. The primary goal is to use this ROM for devising an adaptive duct contraction control strategy that ensured optimal and maximum achievable power output.

To achieve this, we used OpenMDAO [25] along with IPOPT [26] for optimizing control strategies based on the HAHkT responses predicted by the ROM developed in this study. The optimization process aims to maximize power generation by dynamically adjusting pitch and duct CR based on velocity profiles resembling real-time, oscillating inflow conditions. This approach introduces an additional mechanical degree of freedom (DOF) to the HAHkT system, enhancing its ability to extract maximum energy, especially in conditions with relatively slow water freestream speeds.

The OpenMDAO framework with IPOPT optimizer takes into account this SM as a map, the water velocity profile input, and the time rate of change of duct CR (hereinafter referred to as duct CR rate, $\dot{\text{CR}}$) and the time rate change of blade pitch angle (referred to as pitch rate, $\dot{\theta}_b$) constraints in order to provide practical application of these control DOFs considering actuators' mechanical limits in the time variant optimal solution. Unconstrained optimization problems were also explored for comparison.

TABLE 1: Summary of Cases with Applied Constraints

Case	Velocity Profile	ΔCR Con.	ΔPitch Con.
1	$0.4 + 0.3 \cdot \sin(\frac{2\pi}{60} t)$	±0.01175	±3
2	$0.4 - 0.3 \cdot \exp(-\frac{t}{60}) \cdot \sin(\frac{2\pi}{45} t)$	±0.011	±3
3	`numpy.random.seed(42)`	±0.01	±0.5
4	`numpy.random.seed(46)`	±0.025	±5.0

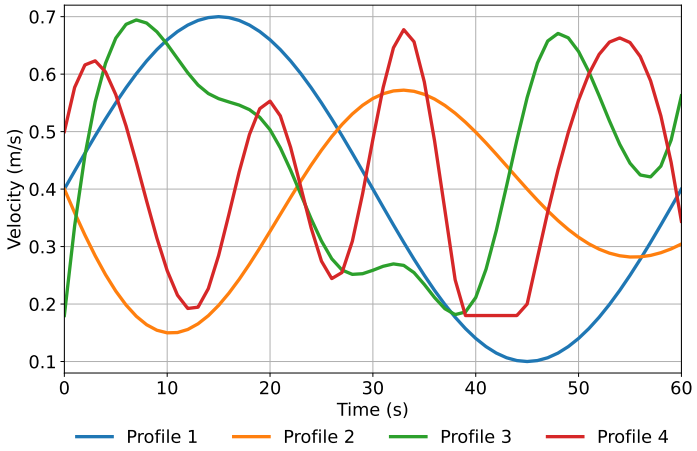

FIGURE 8: Velocity Profiles for Design Optimization

The Gulf Stream core speed is 2 m/s [27], but this exceeds the limits of the SM. Furthermore, most near-shore ocean current speed falls below 1.0 m/s [28]. Therefore, a lower magnitude of velocity profiles were utilized for the optimization tests. The chosen parameters for each design optimization case are shown in Tab. 1. The exact velocity profiles can be seen in Fig. 8. Velocity profiles 1 and 2 are simple sinusoidal and damped sinusoidal respectively. Velocity profiles 3 and 4 are uniformly random generated profiles with Numpy's random seeds 42 and 46 respectively. These profiles represent a range of potential flow

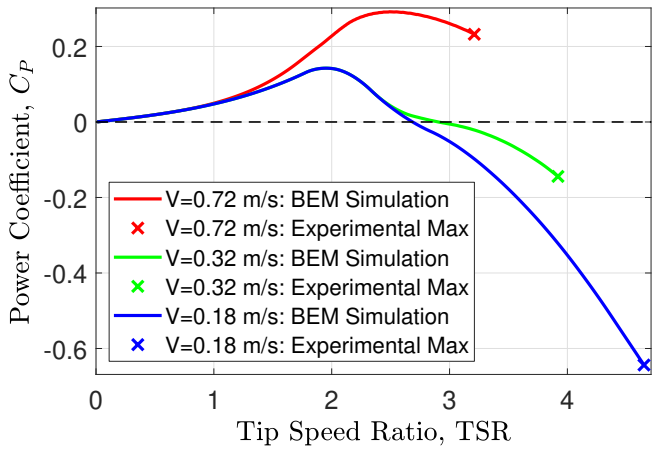

FIGURE 9: QBlade BEMT Simulation Results for Constant Velocity at Collective Pitch −2°

behavior.

The effectiveness and accuracy of the surrogate model as a dynamic ROM will be evaluated by comparing its output against the collected experimental data. Furthermore, the optimization results obtained from OpenMDAO will be assessed against various scenarios where constraints or inflow conditions differ. By comparing the optimizer's paths under these varied conditions, a comprehensive understanding of the system's performance and adaptability can be achieved, ensuring the ducted HAHkT system operates at peak efficiency across a range of scenarios. This streamlined approach marks a significant advancement in the field, aiming to optimize energy production.

3. RESULTS

3.1 Experimental

Four tests for each pitch trial were carried out for each duct CR. The average water speed was determined to be 0.18 m/s. For duct CRs 1, 0.75, and 0.5 the inflow speeds are assumed to be 0.18 m/s, 0.32 m/s, and 0.72 m/s respectively with accordance to continuity. The results for each duct CR corresponding to 1, 0.75, and 0.5 are shown in Figs. 7(a), (b), and (c), respectively. In these plots the mean value, range, and 95 percent confidence interval are identified for each pitch. It can be seen that the design was more effective at a collective pitch of −2° for the the lowest duct CR which corresponds to the highest throat velocity. This shows that the blade design could be altered again such that the 0° produces the most power. These results also produced pitches that were inoperable. It should be noted that a pitch of 12° produced stall for all duct CRs. Combining the results from the three full duct CR tests provides a dynamic representation for power and angular velocity influenced by pitch and duct CR.

3.2 QBlade Simulations

QBlade BEMT rotor simulations were performed at the inflow speed corresponding to continuity from the duct CRs and a collective pitch of −2° since it was the optimal choice for the duct CR that produced the most power experimentally. These BEMT simulations were terminated on the TSR corresponding with the TSR obtained from the maximum angular velocity experimental

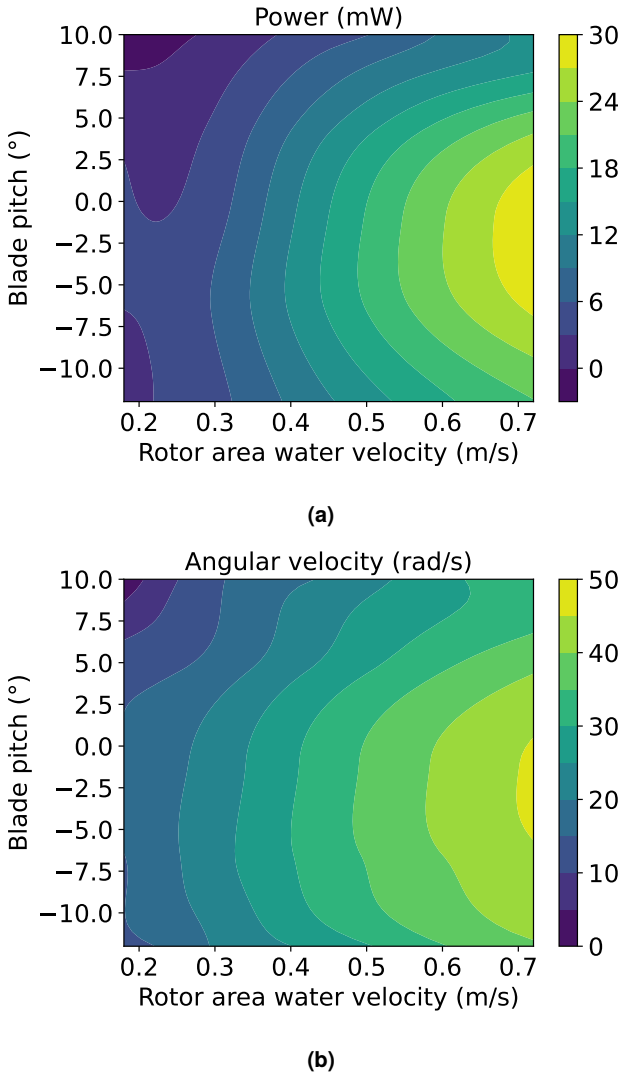

FIGURE 10: Surrogate models produced from experimental data. (a) Power distribution as a function of blade pitch and rotor area velocity. (b) Angular velocity distribution as a function of blade pitch and rotor area velocity.

data for each duct CR. The results for these simulations are shown in Fig. 9 This exhibits that for the rotor design, lower operational TSRs are more optimal but so too are higher inflow speeds. It also verified that imploring the lowest duct CRs produced better power coefficients as inflow remained constant and radial speed varied. The negative power coefficient results show TSR regimes where the rotor consumes energy rather than generating energy, comparable to a propeller. The only way these coefficients of power can be improved is by reducing the drag coefficient which improves the glide ratio by means of either thinning circular sections or increasing the Reynolds number. This opens the door to exploring duct CR values between 0.5 and 0 since the Reynolds number will undoubtedly increase within this regime.

3.3 Adaptive Duct Contraction Control Design

Figures 10(a) and (b) display the surrogate model, SM, created using the open-source surrogate modeling toolbox. This SM

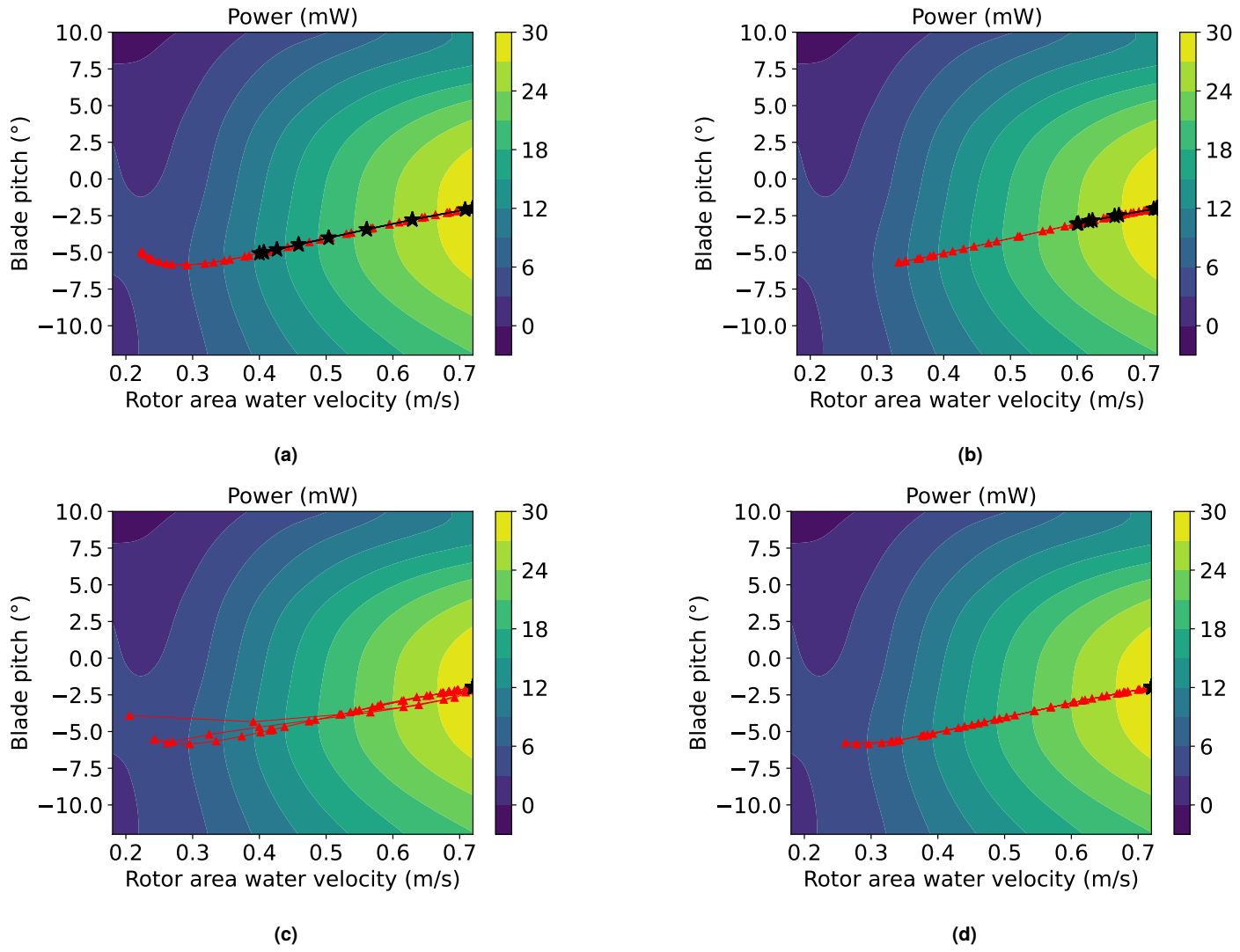

FIGURE 11: Constrained and unconstrained design optimization results for various velocity cases. Contour represents the power in mW for varied rotor area water velocity and blade pitch angle values. (a) Optimal response to sinusoidal velocity profile. (b) Optimal response to damped sinusoidal velocity profile.(c) Optimal response to random uniform velocity profile created with random seed 42. (d) Optimal response to random uniform velocity profile created with random seed 46.

maps power in Fig. 10(a) and angular velocity in (b) as functions of blade angle pitch and rotor area water velocity. The average experimental power results, previously shown in Fig. 7, were the static points utilized to map the behavior and bounds for this model. These maps show that a pitch of −2°and a water velocity of 0.72 m/s generate the maximum power and rotor angular velocity.

Figures 11(a), (b), (c), and (d) depicts the constrained and unconstrained results for the design optimization for each of the cases. The average power output for these case studies are given in Tab. 2. Case 1 and 2 in Figs. 11(a) and (b) both show instances where the duct CR could not bring the water to optimal speed, yet optimal results were always attained for even the slow water speeds. Case 3 and 4 in Figs. 11(c) and (d), where more chaotic velocity functions were implored, the constrained optimization can be seen slightly struggling to stay in the optimal region, while the unconstrained optimizations attained optimality for the entire duration of the simulation. In Figs. 11(a) and (c) the pitch control can be seen responding at very low water speeds in attempt to maximize energy when the duct is fully expanded and cannot further affect the water speed.

TABLE 2: Summary of Optimal Solutions

	Average Power [mW]	
Case	Constrained Case	Unconstrained Case
1	20.30	26.73
2	23.21	28.76
3	20.92	29.15
4	21.50	29.15

Figure 12 illustrates the relationship between overall power production and the levels of rate constraints applied in design optimization case 4. The constraint coefficient, γ, is multiplied

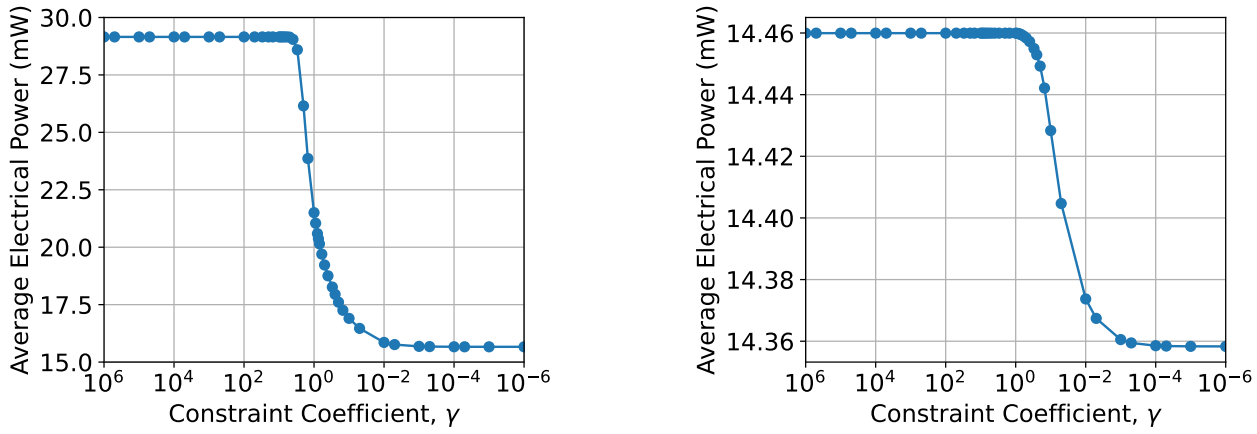

FIGURE 12: Constraint Analysis for Case 4 where the water velocity profile spans the minimum and maximum experimental velocities of 0.18 m/s to 0.72 m/s (a) Duct contraction control and pitch control (b) Pitch-only control and constant contraction ratio of 1

TABLE 3: Summary of Constraint Analysis for Case 4

Case	Average Power (mW)	
	Minimum	Maximum
Duct Contraction and Pitch Control	15.08	29.15
Pitch-only Control and Fixed CR of 1	14.43	14.53

to the lower and upper bounds for duct contraction rate and blade pitch rate, given as:

$$\left|\dot{\mathrm{CR}}\right| \leq \gamma \cdot \dot{\mathrm{CR}}_{\max} \tag{6a}$$

$$\left|\dot{\theta}_{\mathrm{b}}\right| \leq \gamma \cdot \dot{\theta}_{\mathrm{b,max}}, \tag{6b}$$

where $\dot{\mathrm{CR}}$ is the time rate of change of duct CR, $\dot{\theta}_{\mathrm{b}}$ is the time rate of change of blade pitch, and subscript max denotes the predefined limits for the corresponding quantities. When γ approaches to zero, duct contraction and blade pitch control become fixed, making them ineffective. Conversely, as γ approaches infinity, duct contraction and blade pitch control respond immediately to environmental (water flow speed) changes, producing maximum theoretically attainable power. A practical value for γ typically falls within the range of around 1, allowing for finite rates for controller actuation.

Figure 12(a) presents the results of the proposed duct CR control and pitch control. An initial constraint for the DCCS is realistically set which is confirmed with γ of 1 between the minimum and maximum power. Figure 12(b) displays the results of a constant CR of 1 and pitch-only control. A realistic γ for the pitch-only case is around 0.1, between the minimum and maximum power. The DCCS is particularly notable for generating higher average power and offering a broader spectrum of achievable output powers compared to the scenario utilizing only pitch control with a fixed CR of 1. Table 3 provides a comprehensive summary of the constraint analysis, displaying the range of power attainable through the DCCS, which integrates duct contraction and pitch control, as opposed to the range achievable with pitch-only control at a fixed CR of 1. This comparison underscores the substantial impact of incorporating duct contraction control alongside pitch control. In ideal, unconstrained conditions, the DCCS nearly doubles the average power output relative to pitch-only control with a fixed, straight duct. Even under the most stringent constraints, corresponding to a minimum power of 15.08 mW, the DCCS surpasses the unconstrained pitch-only control, which achieves a maximum power of 14.53 mW.

4. CONCLUSIONS

This study introduces a novel adaptive duct CR control strategy for ducted HAHkT systems for relatively lower freestream speed environment, represents a significant advancement in optimizing energy production. By dynamically controlling duct CRs and rotor blade pitch angles simultaneously in response to varying inflow conditions, the design and control strategies presented in this study embodies a forward-thinking approach to maximizing power output in renewable energy systems.

Integration of experimental datasets across different duct CRs and rotor blade pitch angles, along with sophisticated parametric numerical analyses, has led to the development of a refined dynamic model. This model enhances the predictability of system behavior and streamlines the optimization process for duct CR and rotor blade pitch controls, ensuring maximal power extraction in varying inflow conditions. Results from open-channel water flume experiments validated the surrogate model's effectiveness, providing a solid foundation for the proposed adaptive control strategy.

Beyond technical contributions in refining HAHkT design, this research introduces an adaptive framework that addresses the inherent variability in underwater environments. This strategy offers a pathway to achieve higher efficiency in power generation, thereby facilitating the broader adoption of ducted HAHkT systems in locations traditionally considered inadequate due to lower freestream velocity. The DCCS not only enhances performance but also reduces the levelized cost of energy (LCOE), fostering the competitiveness of hydrokinetic energy in the renewable market.

Moreover, the model developed in this study encapsulates a

balanced integration between theoretical modeling and empirical validation, setting a precedent for future research in renewable energy optimization. Promising results underscore the potential for such adaptive strategies to revolutionize the design and operation of energy harvesting systems across wider environmental conditions.

Future work will focus on further refining the dynamic model and adaptive control strategy through extensive simulations and the inclusion of augmented generator control by placing constraints on the angular velocity. Scalability of these results should be realized to fully utilize the higher speeds, particularly in regions, such as the Gulf Stream. By exploring a wider range of inflow conditions and incorporating real-world operational constraints, the aim is to enhance the robustness and applicability of the developed model to large-scale renewable energy projects. The ultimate goal is to contribute to the development of more efficient, reliable, and sustainable renewable energy systems, thereby supporting the global transition towards cleaner and more sustainable energy sources.

REFERENCES

[1] Olabi, A. G. and Abdelkareem, Mohammad A. "Renewable energy and climate change." *Renewable and Sustainable Energy Reviews* Vol. 158 (2022): p. 112111. DOI 10.1016/j.rser.2022.112111.

[2] Neha and Joon, Rambeer. "Renewable energy sources: A review." *Journal of Physics: Conference Series* Vol. 1979 (2021): p. 012023. DOI 10.1088/1742-6596/1979/1/012023.

[3] Soeder, Daniel J. "Fossil Fuels and Climate Change." *Fracking and the Environment: A scientific assessment of the environmental risks from hydraulic fracturing and fossil fuels* (2021): pp. 155–185.

[4] Saini, Gaurav and Saini, Rajeshwer P. "A review on technology, configurations, and performance of cross-flow hydrokinetic turbines." *International Journal of Energy Research* Vol. 43 No. 13 (2019): pp. 6639–6679. DOI 10.1002/er.4625.

[5] Sood, Manoj and Singal, Sunil K. "Development of hydrokinetic energy technology: A review." *International Journal of Energy Research* Vol. 43 No. 11 (2019): pp. 5552–5571. DOI 10.1002/er.4529.

[6] Niebuhr, C. M., van Dijk, M., Neary, V. S. and Bhagwan, J. N. "A review of hydrokinetic turbines and enhancement techniques for canal installations: Technology, applicability and potential." *Renewable and Sustainable Energy Reviews* Vol. 113 (2019): p. 109240. DOI 10.1016/j.rser.2019.06.047.

[7] Chiang, Hsiao-Wei D., Lin, Chen-Yin and Hsu, Chih-Neng. "Design and performance study of an ocean current turbine generator." *International Journal of Turbo & Jet-Engines* Vol. 30 No. 3 (2013): pp. 293–302. DOI 10.1515/tjj-2013-0010.

[8] Jiang, Boxi, Amini, Mohammad Reza, Liao, Yingqian, Martins, Joaquim R. R. A. and Sun, Jing. "Control co-design of a hydrokinetic turbine with open-loop optimal control." *International Conference on Offshore Mechanics and Arctic Engineering*. OMAE2022-81006: p. V008T09A006. 2022. Hamburg, Germany. DOI 10.1115/OMAE2022-81006.

[9] Amini, Mohammad Reza, Jiang, Boxi, Liao, Yingqian, Naik, Kartik, Martins, Joaquim R. R. A. and Sun, Jing. "Control co-design of a hydrokinetic turbine: a comparative study of open-loop optimal control and feedback control." *2023 American Control Conference (ACC)*: pp. 3728–3734. 2023. San Diego, CA. DOI 10.23919/ACC55779.2023.10156550.

[10] Hew, W. R., Saat, F. A. Z. Mohd, Irfan, A. R., Mattokit, E., Rosli, M. A. M., Anuar, F. Shikh, Herawan, S. G. and Syahputra, S. I. A. "Computational fluid dynamics modelling of a hydrokinetic turbine." *AIP Conference Proceedings* Vol. 2347 No. 1 (2021): p. 020195. DOI 10.1063/5.0051477.

[11] Contreras, Leidy Tatiana, Lopez, Omar Dario and Lain, Santiago. "Computational fluid dynamics modelling and simulation of an inclined horizontal axis hydrokinetic turbine." *Energies* Vol. 11 No. 11 (2018): p. 3151. DOI 10.3390/en11113151.

[12] Bilgen, Onur, Wang, Roger, Cao, Yue, Erol, Nazim and Shan, Xin. "A reconfigurable ducted turbine array concept for renewable flow energy harvesting." *AIAA SCITECH 2022 Forum*. AIAA 2022-2222: pp. 1–17. 2022. AIAA, San Diego, CA. DOI 10.2514/6.2022-2222.

[13] Bayat, Saeid, Lee, Yong Hoon and Allison, James T. "Control co-design of horizontal floating offshore wind turbines using a simplified low order model." *Wind Energy Science Conference*: pp. 1–3. Hannover, Germany, May 25–28, 2021.

[14] Saves, Paul, Lafage, Ré'mi, Bartoli, Nathalie, Diouane, Youssef, Bussemaker, Jasper, Lefebvre, Thierry, Hwang, John T., Morlier, Joseph and Martins, Joaquim R. R. A. "SMT 2.0: A Surrogate Modeling Toolbox With a Focus on Hierarchical and Mixed Variables Gaussian Processes." *Advances in Engineering Sofware* Vol. 188 (2024): p. 103571. DOI 10.1016/j.advengsoft.2023.103571.

[15] Alaskari, Mustafa, Abdullah, Oday and Majeed, Mahir H. "Analysis of wind turbine using QBlade software." *IOP Conference Series: Materials Science and Engineering* Vol. 518 No. 3 (2019): p. 032020. DOI 10.1088/1757-899X/518/3/032020.

[16] Marten, David, Peukert, Juliane, Pechlivanoglou, Georgios, Nayeri, Christian and Paschereit, Christian. "QBLADE: An open source tool for design and simulation of horizontal and vertical axis wind turbines." *International Journal of Emerging Technology and Advanced Engineering* Vol. 3 No. 3 (2013): pp. 264–269.

[17] Boretti, Alberto. "State-of-the-art of MW-level capacity oceanic current turbines." *Nonlinear Engineering* Vol. 9 No. 1 (2020): pp. 361–369. DOI 10.1515/nleng-2020-0022.

[18] Batten, W. M. J., Bahaj, A. S., Molland, A. F. and Chaplin, J. R. "Experimentally validated numerical method for the hydrodynamic design of horizontal axis tidal turbines." *Ocean Engineering* Vol. 34 No. 7 (2007): pp. 1013–1020. DOI 10.1016/j.oceaneng.2006.04.008.

[19] Griffin, Austin L. and Lee, Yong Hoon. "Experimental Identification of Reduced Order Model Parameters for Hydroki-

netic Energy System Design." *ASME International Mechanical Engineering Congress and Exposition (IMECE)*. IMECE2023-113489: pp. 1–6. 2023. New Orleans, LA.

[20] Muratoglu, Abdullah and Yuce, Mehmet. "Performance analysis of hydrokinetic turbine blade sections." *Advances in Renewable Energy* Vol. 2 (2015): pp. 1–10.

[21] Nigam, Suyash, Bansal, Shubham, Nema, Tanmay, Sharma, Vansh and Singh, Raj Kumar. "Design and pitch angle optimisation of horizontal axis hydrokinetic turbine with constant tip speed ratio." *MATEC Web of Conferences* Vol. 95 (2017): p. 06004. DOI 10.1051/matecconf/20179506004.

[22] Hasan, Mehedi, El-Shahat, Adel and Rahman, Mosfequr. "Performance investigation of three combined airfoils bladed small scale horizontal axis wind turbine by BEM and CFD analysis." *Journal of Power and Energy Engineering* Vol. 5 No. 5 (2017): pp. 14–27. DOI 10.4236/jpee.2017.55002.

[23] Shahsavarifard, Mohammad, Bibeau, Eric L. and Birjandi, Amir Hossein. "Performance gain of a horizontal axis hydrokinetic turbine using shroud." *OCEANS 2013 - San Diego*: pp. 1–5. San Diego, CA, Septemeber 23–27, 2013. IEEE. DOI 10.23919/OCEANS.2013.6740968. URL https://doi.org/10.23919/OCEANS.2013.6740968.

[24] Barbarić, M. and Guzović, Z. "Investigation of the Possibilities to Improve Hydrodynamic Performances of Micro-Hydrokinetic Turbines." *Energies* Vol. 13 No. 17 (2020): p. 4560. DOI 10.3390/en13174560.

[25] Gray, Justin S., Hwang, John T., Martins, Joaquim R. R. A., Moore, Kenneth T. and Naylor, Bret A. "OpenMDAO: An Open-Source Framework for Multidisciplinary Design, Analysis, and Optimization." *Structural and Multidisciplinary Optimization* Vol. 59 No. 4 (2019): pp. 1075–1104. DOI 10.1007/s00158-019-02211-z.

[26] W achter, Andreas and Biegler, Lorenz T. "On the Implementation of an Interior-Point Filter Line-Search Algorithm for Large-Scale Nonlinear Programming." *Mathematical Programming* Vol. 106 (2006): pp. 25–57. DOI 10.1007/s10107-004-0559-y.

[27] Andres, M. "Spatial and Temporal Variability of the Gulf Stream Near Cape Hatteras." *Journal of Geophysical Research: Oceans* Vol. 126 No. 9 (2021): p. e2021JC017579. DOI 10.1029/2021JC017579.

[28] Haas, Kevin A., Fritz, Hermann M., French, Steven P. and Neary, Vincent S. "Assessment of Energy Production Potential from Ocean Currents along the United States Coastline, Final Project Report." Technical report no. Georgia Tech Research Corporation, Atlanta, GA. 2013. DOI 10.2172/1093367.